Impact of Turbulence Closures and Numerical Errors for the Optimization of Flow Control Devices

J. Labroquère* and R. Duvigneau†

INRIA Sophia Antipolis-Méditerranée - OPALE Project-Team, Sophia-Antipolis, 06902, France

E. Guilmineau‡

LHEEA - CNRS UMR 6598 - Ecole Centrale de Nantes, Nantes, 44321, France

The simulation of turbulent flows including active flow control devices, such as synthetic jets, is still a difficult task. Numerical parameters (grid size, time step, etc.) may have a significant influence on the result, while the choice of the turbulence closure is often critical. In this context, we investigate the use of a Kriging-based global optimization method to determine optimal control parameters. The objective of this study is twofold: firstly, we quantify the impact of some numerical and modeling parameters on the Kriging model constructed using a design of experiment approach. In a second phase, we conduct an optimization process and measure the impact of numerical and modeling errors on the optimal control parameters found. An approach to account for some numerical errors during the optimization is finally presented. The turbulent flow over a backward facing step, including a synthetic jet actuator, is considered as test-case. The time-averaged recirculation length is considered as control criterion, while jet frequency and amplitude are optimized.

I. Introduction

Flow control is an active research area for the last decade, which benefits from the progress of simulation methods in terms of accuracy and robustness, and from the continuous increase of computational facilities. Actuator devices, such as synthetic jets or vortex generators, have proved their ability to modify the flow dynamics and represent a promising way to improve the aerodynamic performance of systems that exhibit massive flow detachment. However, the determination of efficient flow control parameters, in terms of location, frequency, amplitude, etc., is tedious and highly problem dependent.[1,2]

To overcome this issue, the numerical simulation of controlled flows is often considered to determine optimal control parameters, or at least a range of efficient parameters. This task can be carried out in a systematic and parametric way,[2] but the use of an automated optimization procedure is more and more observed.[3–7] Nevertheless, several studies have shown that the simulation of controlled flows is a difficult task, since results may be highly dependent on the turbulence closure used. Comparison between turbulence model is usually carried out for selected control parameters. However the impact of the model on optimal parameters is rarely quantified. Moreover, the numerical assessment should be done carefully because the solution is strongly influenced by the numerical parameters, such as the time step or the grid size. As consequence, the simulation results exhibit modeling and numerical errors, which may lead the optimization process to failure, or to unexpected low efficiency.[8] Surprisingly, this error is almost never taken into account and optimizers use simulation output as if it were exact.

Therefore, this paper is firstly intended to provide a rigorous and systematic assessment of the impact of the turbulence closures and numerical parameters, in the context of the optimization of flow control

*INRIA PhD candidate. E-mail: Jeremie.Labroquere@inria.fr. Tel.: +33 (0)4 92 38 76 15.

†INRIA research associate. E-mail: Regis.Duvigneau@inria.fr. Tel. +33 (0)4 92 38 71 77.

‡CNRS research associate. E-mail: Emmanuel.Guilmineau@ec-nantes.fr. Tel.: +33 (0)2 40 37 16 81.

parameters. Secondly, one explores how to directly take into account errors during the optimization phase, by considering the simulations as noisy observations.

The paper is organized in three main parts: in a first section, simulation methods are described for two flow solvers, a finite-volume cell-centered code for incompressible flows and a hybrid finite-volume / finite-element vertex-centered code for compressible flows. In a second section, we describe the optimization method used, which relies on the iterative construction of a flow database and a corresponding Gaussian Process (GP) model leading the search for optimal parameters. Finally, the third section is devoted to the presentation and analysis of the selected test-case: the flows over a backward facing step. We seek for the optimal frequency and amplitude of a synthetic jet, in order to reduce the flow detachment area as most as possible. In this context, the impact of spatial and temporal discretization, as well as the choice of turbulence closure, is quantified firstly in the context of simulation only, then for optimization purpose.

II. Simulation of controlled flows

II.A. Compressible flow solver

The compressible flow analysis is performed using the NUM3SIS platform developed at INRIA Sophia-Antipolis. The two-dimensional Favre-averaged Navier-Stokes equations can be written in the conservative form:

$$\frac{\partial \boldsymbol{W}}{\partial t} + \frac{\partial F_1(\boldsymbol{W})}{\partial x} + \frac{\partial F_2(\boldsymbol{W})}{\partial y} = \frac{\partial G_1(\boldsymbol{W})}{\partial x} + \frac{\partial G_2(\boldsymbol{W})}{\partial y}, \tag{1}$$

where $\boldsymbol{W}$ are the conservative mean flow variables $(\rho, \rho u, \rho v, E)$, with ρ the density, $\boldsymbol{U} = (u, v)$ the velocity vector and E the total energy per unit of volume. $\boldsymbol{F} = (F_1(\boldsymbol{W}), F_2(\boldsymbol{W}))$ is the vector of the convective fluxes and $\boldsymbol{G} = (G_1(W), G_2(W))$ the vector of the diffusive fluxes. The pressure p is obtained from the perfect gas state equation $p = (\gamma - 1)(E - \frac{1}{2}\rho \| \overrightarrow{U} \|^2)$ where $\gamma = 1.4$ is the ratio of the specific heat coefficients.

Provided that the flow domain Ω is discretized by a triangulation $\mathcal{T}_h$, a discretization of equation (1) at the mesh node s_i is obtained by integrating (1) over the volume C_i, that is built around the node s_i by joining the centers of the triangles containing s_i and midpoints of the edges adjacent to s_i:

$$Vol_i \frac{\partial W_i}{\partial t} + \sum_{j \in N(i)} \Phi(W_i, W_j, \overrightarrow{\sigma}_{ij}) = \sum_{k \in E(i)} \Psi_k, \tag{2}$$

where W_i represents the cell averaged state and Vol_i the volume of the cell C_i. $N(i)$ is the set of the neighboring nodes and $E(i)$ the set of the neighboring triangles. $\Phi(W_i, W_j, \overrightarrow{\sigma}_{ij})$ is an approximation of the integral of the convective fluxes over the boundary ∂C_{ij} between C_i and C_j, which depends on W_i, W_j and $\overrightarrow{\sigma}_{ij}$ the integral of a unit normal vector over ∂C_{ij}. The convective fluxes are evaluated using upwinding, according to the approximate Riemann solver HLLC.[9] A high order upwind scheme is obtained by reconstructing the physical variables at the midpoint of $[s_i s_j]$ using W_i, W_j and the upwind gradient (β-scheme), before the fluxes are evaluated. Ψ_k is the contribution of the triangle k to the diffusive terms, according to a classical P1 description of the flow fields.

An implicit dual-time stepping procedure is used for the time integration of (2). A classical three-step backward scheme ensures a second-order accurate discretization of the unsteady term. A first-order backward scheme is employed for the pseudo-time integration. The linearization of the numerical fluxes provides the following integration scheme:

$$\left((\frac{Vol_i}{\Delta t} + \frac{Vol_i}{\Delta \tau})\, Id + J_i^p \right) \delta W_i^{p+1} = - \sum_{j \in N(i)} \Phi_{ij}^p + \sum_{k \in E(i)} \Psi_k^p - \frac{3}{2}\frac{Vol_i}{\Delta t}\delta W_i^n + \frac{1}{2}\frac{Vol_i}{\Delta t}\delta W_i^{n-1} \tag{3}$$

with:

$$\delta W_i^{p+1} = (W_i^{n+1})^{p+1} - (W_i^{n+1})^p \qquad \delta W_i^n = (W_i^{n+1})^p - W_i^n \qquad \delta W_i^{n-1} = W_i^n - W_i^{n-1} \tag{4}$$

J_i^p is the Jacobian matrix of the convective and diffusive terms. $\Delta\tau$ is the pseudo-time step. For the computation of the convective Jacobian, we employ the first-order flux of Rusanov,[10] while the diffusive Jacobian is computed exactly. The right hand side of (3) is evaluated using high order approximations. The resulting integration scheme provides a second-order solution in space and time. The linear system is

inverted using a SGS method.

Transport equations for turbulence closures are solved in a similar fashion, separately from mean flow equations. Turbulent variables are coupled to flow variables using the Boussinesq eddy-viscosity assumption.

II.B. Incompressible flow solver

The incompressible flow study is carried out with the ISIS-CFD solver, developed at LHEEA and available as a part of the FINE^{TM}/Marine computing suite. It solves incompressible Unsteady Reynolds-Averaged Navier-Stokes (URANS) equations. The solver is based on finite-volume method to build the spatial discretization and solves the conservation equations with a face-based cell-centered approach.

Within this framework, the incompressible conservation laws under isothermal conditions are written as

$$\frac{\partial}{\partial t}\int_V \rho dV + \int_S \rho \boldsymbol{U}\cdot\boldsymbol{n}dS = 0, \tag{5}$$

$$\frac{\partial}{\partial t}\int_V \rho U_i dV + \int_S \rho U_i \boldsymbol{U}\cdot\boldsymbol{n}dS = \int_S (\tau_{ij}I_j - pI_i)\cdot\boldsymbol{n}dS, \tag{6}$$

where V is the domain of interest or control volume, bounded by the closed surface S with a unit normal vector $\boldsymbol{n}$ directed outward. $\boldsymbol{U}$ and p represent, respectively, the velocity and pressure fields. τ_{ij} are the components of the viscous stress tensor, whereas I_j is a vector whose components are zero, except for the j^{th} component which is equal to unity.

All flow variables are stored at geometric centers of the arbitrary shaped cells. Surface and volume integrals are evaluated according to second-order accurate approximations by using the values of integrand that prevail at the center of the face f, or cell C , and neighbor cells C_{nb}. The various fluxes appearing in the discretized equations (5) and (6) are built using the Gamma Differencing Scheme (GDS).[11,12] Some other flux determination methods, as centered, upwind or hybrid schemes, are implemented in ISIS-CFD. More can be found in Duvigneau and Visonneau[13] and more recently in Queutey and Visonneau.[12] A pressure equation is obtained in the spirit of the Rhie and Chow SIMPLE algorithm.[14] As for the compressible solver, unsteady terms are solved using a dual-time stepping approach.

In the case of turbulent flows, additional transport equations for modeled variables are discretized and solved using the same principles.

II.C. Turbulence closures

Various turbulence closures are implemented in the flow solvers as linear and non-linear eddy-viscosity based models. For this study, a compressible version of Spalart-Allmaras model is used in NUM3SIS, while various incompressible models are used for ISIS-CFD. Their main characteristics are described below.

II.C.1. Spalart-Allmaras closure

The Spalart-Allmaras closure is a one-equation closure calibrated on simple flows which is intensively used in aerodynamics. It provides satisfactory results on attached flows and gives a better description of velocity fields for detached flows than zero-equation models. Several versions and variants of this model, including curvature corrections, have been developed since the original version was written. The details of the model are not described here, but the implemented compressible[15] and incompressible[16] versions correspond to the standard Spalart-Allmaras model.

II.C.2. k-ϵ Launder-Spalding and k-ω-SST Menter closures

The k-ε Launder-Spalding[17] and the k-ω models are two-equation turbulence closures. The aim of these closures is to predict the length scale and the time reversal of the largest turbulence eddies in the flow. To determine these characteristics, the k-ε model is based on solving the turbulent energy k and the dissipation rate ε while the k-ω uses the turbulent energy k and the characteristic frequency ω of the largest eddies. It is well known that the simple k-ω closure is sensitive to boundary conditions, but can be integrated to the wall, while the k-ε closure is not sensitive to boundary conditions, but cannot be integrated to the wall unless using damping functions. By taking both advantages of the k-ε and k-ω closures, the k-ω-SST from

Menter closure[18] is deduced by mixing the k-ε closure far away from walls to k-ω closures close to the walls. The coefficients of the closures are calibrated on simple flows at equilibrium.

The application domain for these two models is more general than the Spalart-Allmaras closure, but still limited by the linear Boussinesq assumption. The baseline closures of k-ε Launder-Spalding and k-ω-SST Menter are used in this study.

II.C.3. Algebraic Stress Models (ASM)

Explicit and Implicit Algebraic Stress Models belong to the larger class of Algebraic Stress Models. They are based on an extension of the linear Boussinesq assumption, designed to add anisotropic behaviors to two-equation closures. These models are non-linear and are built upon a full Reynolds Stress estimation, on the basis of a transport equation for a two-equation closure.

Contrary to two-equation closures, the Algebraic Stress Models can handle negative production of energy, rotational effects, etc. Furthermore, unsteady flows are characterized by a misalignment between the anisotropy tensor and the strain tensor.[19] As a consequence, two-equation closures are not able to predict these features, due to their linear nature, while Algebraic Stress Models can better predict such complex flows. Finally, an advantage of the formulations of Algebraic Stress Models is that they do not need to be calibrated.

In ISIS-CFD, the Explicit Algebraic Stress Model based on the k-ω closure by Gatski & Speziale[20] with a near-wall formulation[21] is implemented.

II.D. Actuators models

In this study, we consider actuations based on synthetic jets. For both solvers, the actuation is implemented as boundary conditions. In the case of incompressible flows, the velocity is imposed on the jet boundary and is defined as:

$$\boldsymbol{U} = U_j A(\mathbf{x}) \sin(\omega t)\ \boldsymbol{d_j}$$

with A($\mathbf{x}$) a unit profile function, U_j the amplitude, ω the angular frequency and $\boldsymbol{d_j}$ the direction of the jet. In this study, $A(\mathbf{x})$ is a sine squared function and $\boldsymbol{d_j}$ is normal to the boundary.

For the compressible flow solver, the velocity is imposed in a similar fashion. Additionally, other variables are extrapolated from the interior of the domain.[22]

III. Optimization of control devices

When dealing with turbulent unsteady flows, the main issue for optimization is the computational burden. The evaluation of the cost function gradient using an adjoint approach is highly complex and the non-linear underlying phenomena may yield multimodality. Furthermore, the optimization process may fail due to simulation errors (discretization, convergence, etc.), which make the evaluations noisy. To address these issues, the use of meta-models based on simulation results seems to be a promising approach.[23] In particular, the present work is focused on the Efficient Global Optimization (EGO) algorithm.

The EGO is a global optimization algorithm that makes use of a stochastic process model to drive the optimization.[24] As a first design of experiment phase, an initial database covering the bounded search space is generated from simulations. This database contains obviously the cost function values, but may also gather the error estimated for each evaluation. A stochastic model is constructed using this database, which allows to predict the cost function value in term of expectancy and variance at any point of the search domain. According to these predictions, the most interesting points are selected by means of a merit function. Once evaluated, the corresponding cost function values and the error estimations are added to the database. This process is repeated until convergence, as illustrated on Fig. 1.

III.A. Gaussian Process model

Gaussian Process models (also known as kriging models) belong to response surface methods, that allow to predict a function value f at a given point x, on the basis of a set of observed values $\boldsymbol{F_N} = \{f_1, f_2, \ldots, f_N\}$ at some points $\boldsymbol{X_N} = \{x_1, x_2, \ldots, x_N\} \subset \mathbb{R}^d$. $\boldsymbol{F_N}$ is assumed to be one realization of a multivariate Gaussian

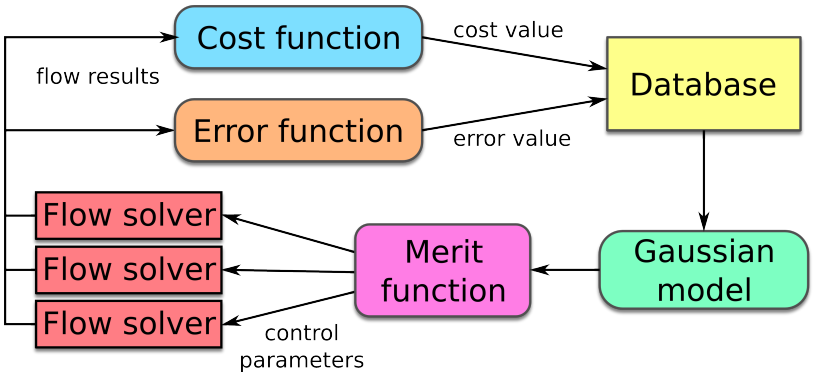

Figure 1. Efficient Global Optimization loop.

process which have a joint Gaussian distribution

$$p(\boldsymbol{F_N}|C_N, \boldsymbol{X_N}) = \frac{\exp\left(-\frac{1}{2}\boldsymbol{F_N}^\top C_N^{-1}\boldsymbol{F_N}\right)}{\sqrt{(2\pi)^N \det(C_N)}}, \tag{7}$$

for any collection of inputs $\boldsymbol{X_N}$. C_N is the $N \times N$ covariance matrix, whose elements C_{mn} give the correlation between the function values f_m and f_n obtained at points x_m and x_n. We assume that these values are correlated, since they correspond to underlying physical phenomena. This is expressed in terms of a correlation function k, i.e., $C_{mn}(x_m, x_n; \Theta) = cov(f_m, f_n) = k(x_m, x_n; \Theta)$ with Θ a set of hyper-parameters that are supposed to be known in the following.

Now, we suppose that we would like to evaluate the function value at a new point x_{N+1}. From Eq. (7), the $(N+1)$-variable Gaussian process has a joint probability density of

$$p(\boldsymbol{F_{N+1}}|C_{N+1}, \boldsymbol{X_{N+1}}) = \frac{\exp\left(-\frac{1}{2}\boldsymbol{F_{N+1}}^\top C_{N+1}^{-1}\boldsymbol{F_{N+1}}\right)}{\sqrt{(2\pi)^{N+1} \det(C_{N+1})}}. \tag{8}$$

To predict the unknown function value f_{n+1} given the data $\boldsymbol{F_N}$, one uses the conditional probabilities rule $p(A|B) = p(A,B)/p(B)$:

$$p(f_{N+1}|(\boldsymbol{X_N}, \boldsymbol{F_N}), C_N, x_{N+1}) = \frac{p(\boldsymbol{F_{N+1}}|C_N, \boldsymbol{X_{N+1}})}{p(\boldsymbol{F_N}|C_N, \boldsymbol{X_N})}. \tag{9}$$

After some calculations,[25] we obtain that the probability density for the function value at the new point is

$$p(f_{N+1}|(\boldsymbol{X_N}, \boldsymbol{F_N}), C_N, x_{N+1}) \propto \exp\left[-\frac{(f_{N+1} - \hat{f}_{N+1})^2}{2\hat{\sigma}^2_{f_{N+1}}}\right],$$

where

$$\hat{f}_{N+1} = \boldsymbol{k_{N+1}}^\top C_N^{-1}\boldsymbol{F_N}, \qquad \hat{\sigma}^2_{f_{N+1}} = \kappa - \boldsymbol{k_{N+1}}^\top C_N^{-1}\boldsymbol{k_{N+1}}, \tag{10}$$

with $\kappa = k(x_{N+1}, x_{N+1}; \Theta)$ and $\boldsymbol{k_{N+1}} = [k(x_1, x_{N+1}; \Theta), \ldots, k(x_N, x_{N+1}; \Theta)]^T$.

Thus, the probability density for the function value at the new point x_{N+1} is also Gaussian with mean $\hat{f}_{N+1}$ and standard deviation $\hat{\sigma}_{f_{N+1}}$. Therefore, the most likely value at the new point x_{N+1} is $\hat{f}_{N+1}$. This value will be considered as the prediction of the kriging model. The variance $\hat{\sigma}^2_{f_{N+1}}$ can be interpreted as a measure of uncertainty in the value prediction. The function value can be expected to vary in some range like $[\hat{f} - 3\hat{\sigma}, \hat{f} + 3\hat{\sigma}]$.

III.B. Correlation functions

The choice of the correlation function k is critical for the model, as it contains all the prior hypotheses, including for example regularity, symmetry, periodicity, etc. The correlation function must *a priori* reflect the characteristics of the output of the computer code.

We use here the Matérn class of covariance stationary kernels, which gives a family of correlation functions of different smoothness. More specifically, the following multidimensional correlation function is employed:

$$k(\boldsymbol{x}, \boldsymbol{x'}; \boldsymbol{\Theta}) = \theta_1 \prod_{i=1}^{d} e^{-\left(\frac{|\boldsymbol{x}-\boldsymbol{x'}|}{r_i}\right)^2} + \theta_2, \tag{11}$$

with $\boldsymbol{\Theta} = \{\theta_1, \theta_2, r_1, r_2, ..., r_d\}$ the set of hyper-parameters to be determined. Practical studies have shown that the use of a non-isotropic scaling is beneficial for the problems considered here. The parameter θ_1 scales this correlation. In the second term, θ_2 gives an offset of the function values from zero. The parameters r_i represent the anisotropic distance at which the correlation decays.

III.C. Hyperparameters determination in Bayesian framework

The Bayesian framework allows to make inference with prior knowledge about the cost function. This framework[26] is used to determine the hyper-parameters Θ in the correlation function.

We want the constructed model to be as consistent as possible with the observed data. Therefore, hyper-parameters are determined by maximizing the probability density function of the observed data, or equivalently by minimizing the log-likelihood function given by:

$$\mathfrak{L} = -\log p(\boldsymbol{F_N}|\boldsymbol{X_N}, C_N, \Theta) = \boldsymbol{F_N}^\top C_N^{-1} \boldsymbol{F_N} + \log\det(C_N). \tag{12}$$

This function is known to be multi-modal; hence an evolution strategy is employed for this work, that has the capability to avoid local minima.

III.D. Merit functions

Once the model is constructed, it is used to locate the most interesting value of the cost function. The naive choice of the minimum of the model may yield to non-optimum or even non-stationary points.[27] Therefore, the new point to be evaluated is chosen by minimizing or maximizing a merit function, which makes use of the variance of the model. A comprehensive review of the different merit functions to locate the optimum for deterministic functions is given by Jones.[27] Four different merit functions are used in this study, which use the variance of the model to reach the global optimum.

Lower bound (LB): The simplest criterion is the minimization of the lower bound. This merit function is defined as:

$$LB(x) = \hat{f}(\boldsymbol{x}) - \rho\hat{\sigma}(\boldsymbol{x}) \tag{13}$$

where ρ is a constant typically chosen to be equal to 0, 1 or 2. Note that when $\rho = 0$, the criterion reduces to the minimization of the meta-model only.

Probability of Improvement (PI): Maximizing the probability of improvement consists in choosing a point which maximizes the probability of obtaining a value better than a given target. To do so, a target value is set, such that $T < f_{min}$ with $f_{min} = \min_{1\leq i\leq N} f(\boldsymbol{x_i})$. This merit function is finally computed by:

$$PI(\boldsymbol{x}) = \Phi\left(\frac{T - \hat{f}(\boldsymbol{x})}{\hat{s}(\boldsymbol{x})}\right), \tag{14}$$

where $\Phi(y) = \frac{1}{2}(1 + \mathrm{erf}(y/\sqrt{2}))$ is the cumulative distribution function of the standard normal distribution. As for LB, several target values T can be chosen.

Expected Improvement (EI): The most popular strategy is the maximization of the Expected Improvement (EI).[24] This approach consists in locating the point $\boldsymbol{x}$ at which the maximum reduction of the cost function can be expected. The improvement obtained by evaluating Y at the point $\boldsymbol{x}$ is defined as:

$$I := \max(f_{\min} - Y(\boldsymbol{x}), 0). \tag{15}$$

If we assume that the function value is the realization of a random variable with mean $\hat{f}(\boldsymbol{x})$ and standard deviation $\hat{\sigma}(\boldsymbol{x})$, the probability of reducing its value by an amount I is given by:

$$\frac{1}{\sqrt{2\pi}\hat{\sigma}(\boldsymbol{x})} \exp\left[-\frac{(f_{min} - I - \hat{f}(\boldsymbol{x}))^2}{2\hat{\sigma}(\boldsymbol{x})^2}\right]. \tag{16}$$

Then, the EI criterion is the expected value of I:

$$EI(\boldsymbol{x}) = \int_{I=0}^{I=\infty} I \left\{ \frac{1}{\sqrt{2\pi}\hat{\sigma}(\boldsymbol{x})} \exp\left[-\frac{(f_{min} - I - \hat{f}(\boldsymbol{x}))^2}{2\hat{\sigma}(\boldsymbol{x})^2}\right] \right\} dI. \tag{17}$$

After an integration by part, it is shown that:

$$EI(\boldsymbol{x}) = \hat{\sigma}(\boldsymbol{x})[u\Phi(u) + \phi(u)], \quad u(\boldsymbol{x}) = \frac{f_{min} - \hat{f}(\boldsymbol{x})}{\hat{\sigma}(\boldsymbol{x})}, \tag{18}$$

where $\phi(y) = \frac{1}{\sqrt{2\pi}} \exp(-y^2/2)$ is the standard normal distribution.

Augmented Expected Improvement (AEI): The main drawback of the EI criterion is that the minimum f_{min} is not exactly known in presence of noise. The Augmented Expected Improvement[28] is based on two modifications in case of noisy functions. First, instead of using the minimum f_{min}, it uses a surrogate, addressing the problem that f_{min} is not exactly known. The used surrogate is $T = \hat{f}(\boldsymbol{x}^{**})$ with $\boldsymbol{x}^{**}$ (*effective best solution*) the minimum of $\hat{f} + \hat{\sigma}$ over the over the current database. Then, a penalty term is introduced in order to take into account the error for the next evaluation τ_{N+1}. This penalty enhances exploration by penalizing points with small variance $\hat{\sigma}^2$ with respect to noise τ_{N+1}^2. Finally, the AEI criterion becomes:

$$AEI(\boldsymbol{x}) = EI_T(\boldsymbol{x}) \times \left(1 - \frac{\tau_{N+1}}{\sqrt{\hat{\sigma}(\boldsymbol{x})^2 + \tau_{N+1}^2}}\right), \qquad EI_T(\boldsymbol{x}) = \hat{\sigma}(\boldsymbol{x})[u\Phi(u) + \phi(u)], \quad u(\boldsymbol{x}) = \frac{T - \hat{f}(\boldsymbol{x})}{\hat{\sigma}(\boldsymbol{x})} \tag{19}$$

The AEI criterion has exhibited the best results for the optimization of noisy functions among many merit functions.[29]

IV. Test-case

IV.A. Backward facing step

The backward facing step is a well known test-case, studied by many researchers experimentally as well as numerically. This test-case is selected here to provide detached flows with a simple geometrical configuration. The configuration defined by Driver and Seegmiller[30] is used in this study. It has been documented using incompressible[31,32] as well as compressible[33] flows.

IV.A.1. Configuration

The backward-facing step geometry including a control device is defined on the figure 2. The geometry and parameters are taken from the Driver case: $h = 0.0127$m, $U_{ref} = 44.2$m/s, $M_{ref} = 0.128$, the Reynolds number based on the boundary layer momentum thickness prior to the step is set to $Re_\theta = 5000$ and the boundary layer thickness at the inlet is $\delta_{BL} = 0.019$m. The control device is a suction / blowing jet with a diameter of $h/10$ and is located at $h/50$ from the step.

Three different meshes have been designed for this particular configuration. In the incompressible case, the coarse, medium and fine mesh respectively contains 29778, 45805 and 77064 nodes. In the compressible

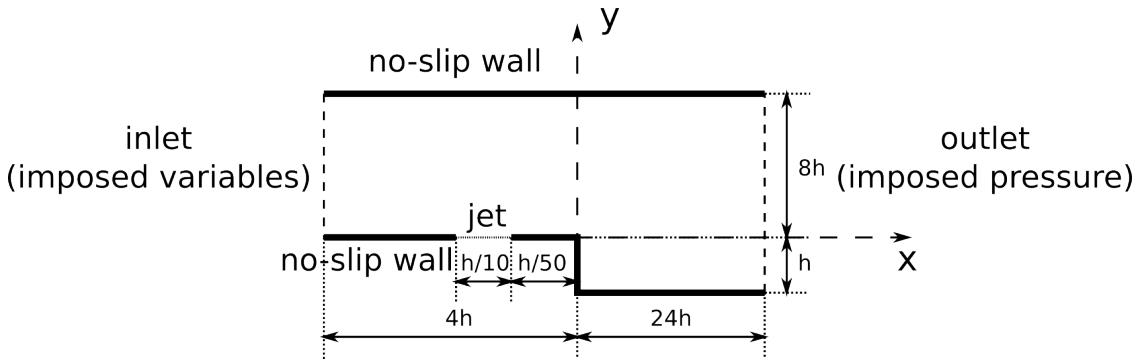

Figure 2. Backward-facing step configuration.

case, the mesh respectively contains 16575, 38235 and 70538 nodes. In all cases, the boundary layer is refined at the wall to fulfill the $y^+ < 1$ criterion at all time steps.

As well, three different time steps based on the jet frequency are selected. The large, medium and small time steps are defined so that one period contains respectively 64, 128 and 256 time steps.

In a previous work,[34] starting from the steady solution of the uncontrolled flow, it has been noticed that the transient effect has vanished after 0.025s. Therefore, the time averaging process starts at 0.035s and last for 4 full periods.

IV.A.2. Optimization parameters

The objective function for this test-case is the recirculation length of the time-averaged flow. A post treatment locates where the wall shear stress vanishes. As design parameters, we consider the jet amplitude and frequency, which are allowed to vary in the following intervals: $4\text{m/s} \leq U_{jet} \leq 50\text{m/s}$ and $50\text{Hz} \leq f_{jet} \leq 1000\text{Hz}$.

V. Impact of parameters on simulation flow results

Several studies on the assessment of turbulence closures for backward facing step configurations have been carried out for the last years.[33,35] Simulations are validated by comparing mean flow velocity profile distribution, pressure coefficient and bubble recirculation length past the step. With control devices, the same criteria are usually considered but only a few couples of blowing frequencies and amplitudes are chosen in most studies. In the perspective of optimization of flow control devices, a more global assessment is targeted.

First of all, to quantify the impact of turbulence models, meta-models built using different closures are compared on the same grid. Then, a grid and time step refinement is done to estimate the discretization errors, for all the turbulence closures. Finally, a comparison between the compressible code NUM3SIS and the incompressible code ISIS-CFD is conducted, for a fixed turbulence closure. For all cases, the initial database is composed of 16 design points determined by an optimized Latin Hypercube Sampling (LHS).

V.A. Impact of turbulence closure

It is well known that turbulence models have a huge impact on detached flow simulations. Nevertheless, the capability to obtain similar trends for the optimum actuation is investigated here. This study is carried out using the medium grid, with the ISIS-CFD flow solver. Four turbulence models are tested: the Spalart-Allmaras (SA), k-ε Launder-Sharma (KE-LS), k-ω-SST Menter (KW-SST-MENTER) and quadratic explicit algebraic stress model (KW-NE-EASM).

V.A.1. Flow without control

At first, we compare the results for the flow without actuation. It is used to initialize the simulation of the controlled flow over the backward-facing step. The velocity streamlines for the different turbulence closures

are shown on the Fig 3. The effect of turbulence closure is obvious, even for the steady non-controlled

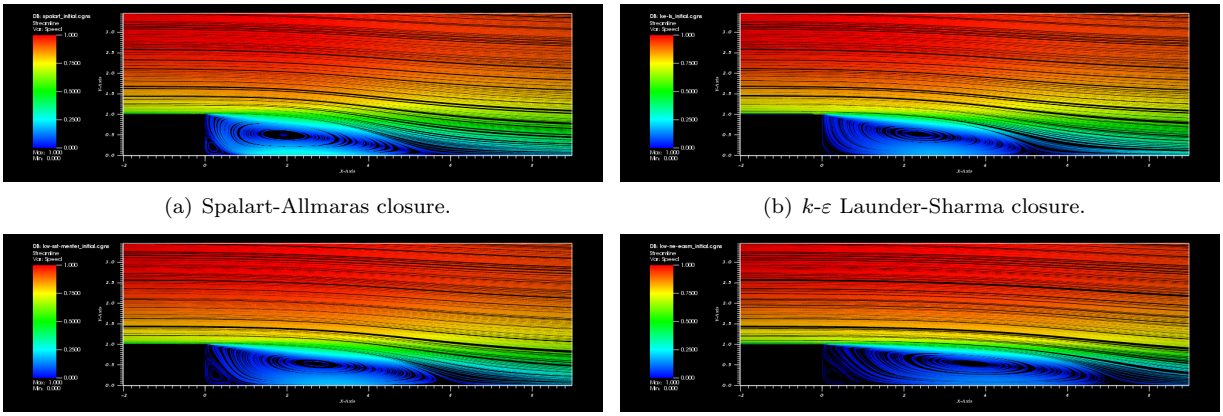

(a) Spalart-Allmaras closure.

(b) k-ε Launder-Sharma closure.

(c) k-ω-SST Menter closure.

(d) k-ω-ne-easm closure.

Figure 3. Comparison of velocity streamlines for different turbulence closures for the flow over the backward facing step without control.

flow. While the shapes of the recirculation bubble are close for the Spalart-Allmaras, k-ε Launder-Sharma and k-ω-SST Menter closures, the quadratic explicit algebraic stress model predicts a significantly longer recirculation bubble. On the Fig. 4, the velocity profiles at different locations are represented. As well, the

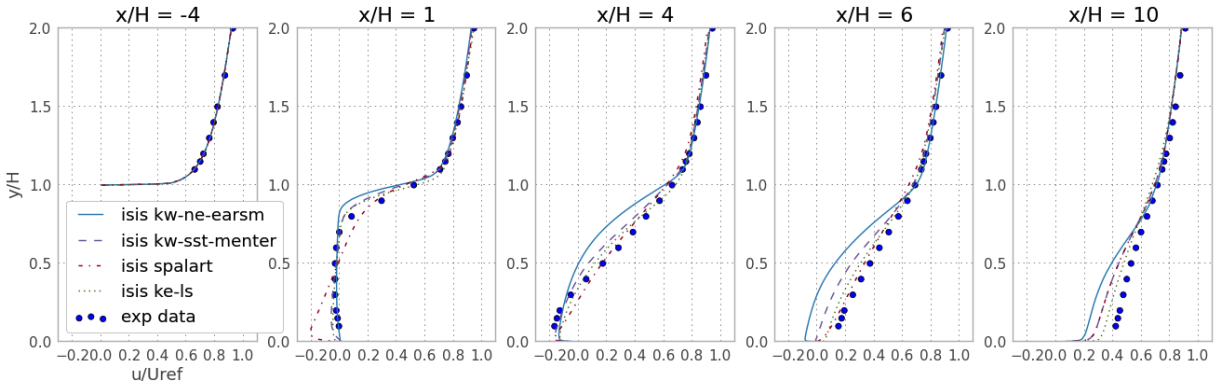

Figure 4. Initial velocity profiles at $x = -4$, $x = 1$, $x = 4$,$x = 6$ and $x = 10$ for different turbulence closures for the flow over the backward facing step without control.

table 1 gives the recirculation length for the different models.

Experimental	Spalart-Allmaras	k-ε Launder-Sharma	k-ω SST Menter	k-ω-ne-easm
6.26	6.05	5.41	6.37	7.56

Table 1. Comparison of recirculation length l/h computed against the experimental results from Driver and Seegmiller.

As seen, the k-ω SST Menter is the closest one to the experimental recirculation length value while the Spalart-Allmaras and k-ε Launder-Sharma underestimate it and the k-ω-ne-easm overestimates the recirculation bubble length. The Spalart-Allmaras closure has the worst behavior concerning the velocity profiles.

V.A.2. Flow with control

The meta-models for the different turbulence closures are presented on Fig. 5. These models were generated with simulations including 256 time steps per period on the medium grid and for a reduction of 3 orders for the non linear residuals. Effect of discretization error are further studied.

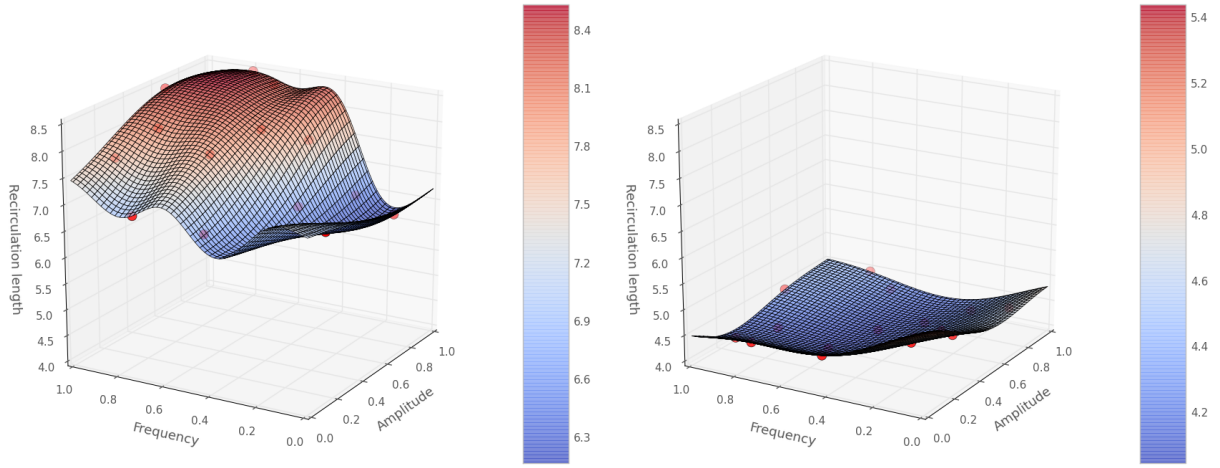

(a) Spalart-Allmaras closure.

(b) k-ε Launder-Sharma closure.

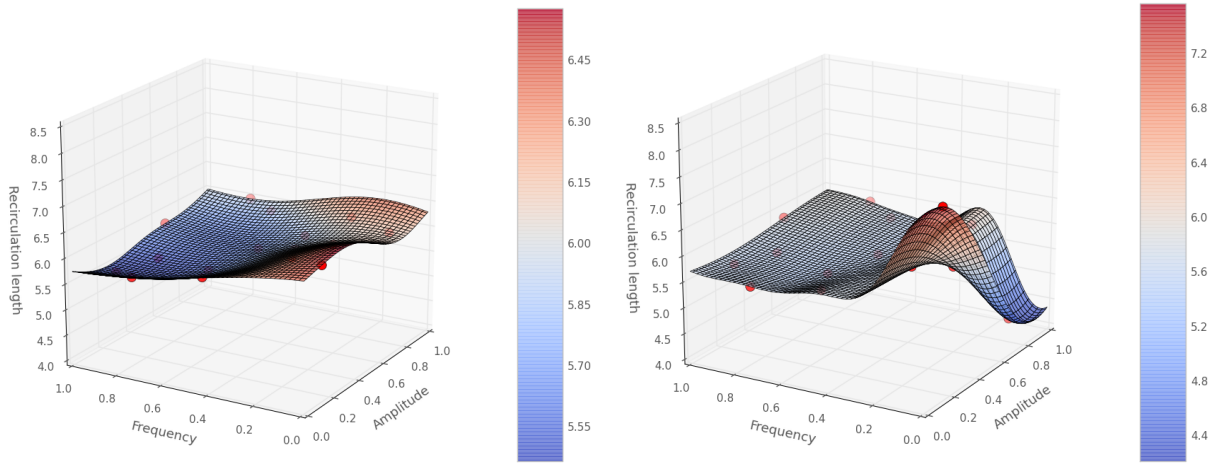

(c) k-ω-SST Menter closure.

(d) k-ω-ne-easm closure.

Figure 5. Influence of turbulence closures on the recirculation length.

As can be observed, the trend of the meta-model is significantly dependent on the closure chosen. The Spalart-Allmaras closure provides a model whose shape is very different from the other ones. The k-ω-SST Menter, k-ε Launder-Sharma and k-ω-ne-easm closures agree for the medium and high frequencies, while the very low frequencies significantly differ.

The Fig 6 compares the vorticity for the k-ω-SST Menter and k-ω-ne-easm models. The selected design point corresponds to a non dimensional amplitude of 0.8 and a frequency of 0.0666667 ($40.8m/s$ and a frequency of $113.333Hz$). The non linearities of the k-ω-ne-easm turbulence model are observed on the instantaneous vorticity of the flow. The k-ω-SST Menter is more diffusive and the k-ω-ne-easm tends to be more rotational than its counterpart.

V.B. Impact of discretization errors

The discretization errors for unsteady simulations is due to the grid size and the time step. The k-ω-ne-easm turbulence closure is used for this study.

V.B.1. Grid refinement

To measure the effects of the grid size on the meta-model, three grids are considered, with a fixed number of 256 time steps per period and a reduction of 4 orders of non linear residuals. The different meta-models

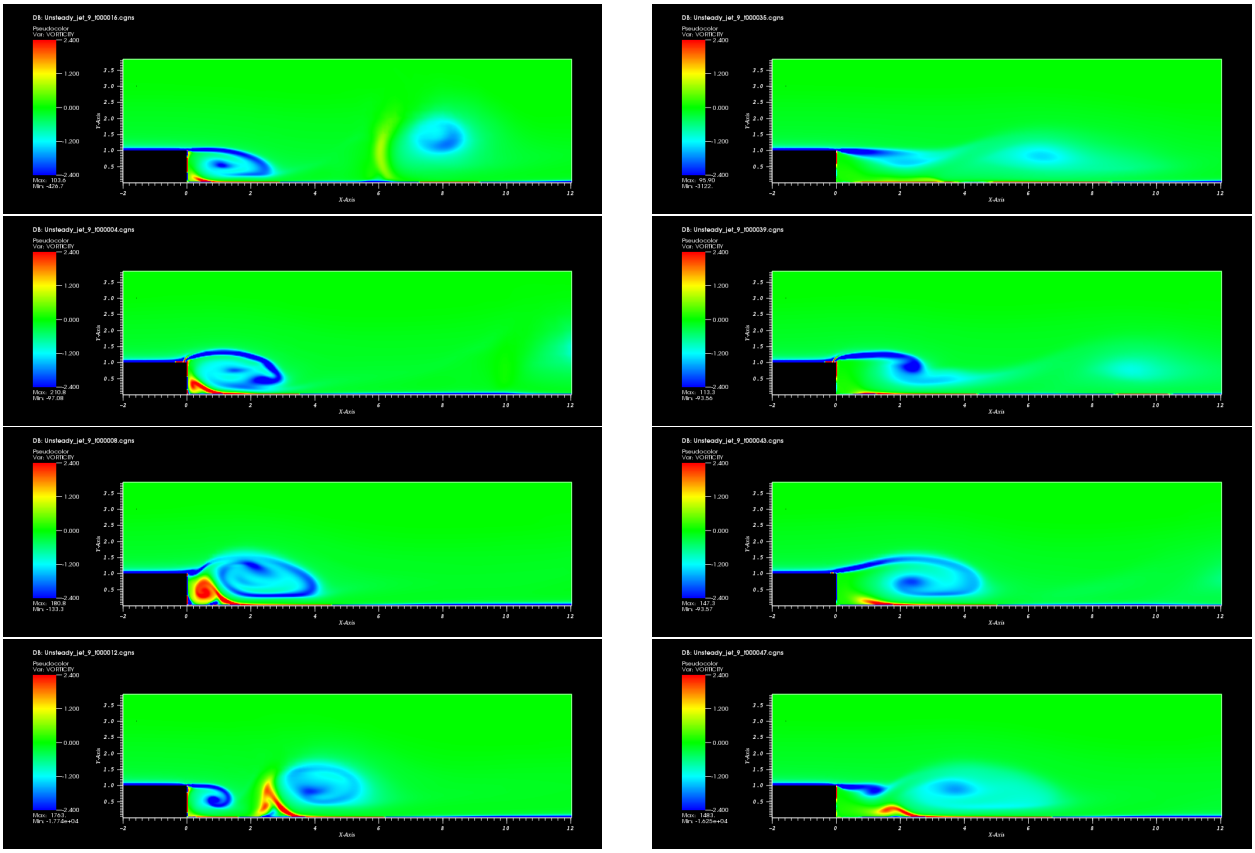

Figure 6. Comparison of the vorticity for k-ω-ne-easm (left) and k-ω-SST Menter (right) turbulence closure with 256 time steps by periods and the medium mesh. The current actuation point has an amplitude of $40.8m/s$ and a frequency of $113.333Hz$. From top to bottom, the jet angular phase is $\omega \approx 0$, $\omega \approx \frac{\pi}{2}$, $\omega \approx \pi$ and $\omega \approx \frac{3\pi}{2}$.

obtained using the three grids can be compared on Fig. 7. Results look quite similar for all the grids. One can notice that the effects of medium and high frequencies actuation is better captured when the grid is refined. The grid size do not exhibit a strong influence on low frequencies. The overall meta-model shape is not really sensitive to grid refinement as the effective control in medium frequencies and low frequencies is still located around the same location.

V.B.2. Time step refinement

To quantify the effects of the time step, three different discretization of 64, 128 and 256 time steps per period are selected, with the fine grid and a reduction of non linear residuals of 4 orders. The meta-models shown on Fig. 8, do not look different. Surprisingly, change of the time step has not a strong influence on the meta-model shape.

V.C. Iterative error

Dual time stepping method implies the convergence of the flow equations at each time step. Here, the effect of the reduction of non linear residuals on the meta-model is quantified for 1, 2 and 4 orders as stopping criterion. The medium grid, with 256 time steps per period is selected. The Fig. 9 shows the different meta-models obtained. The order of convergence has a huge effect on the meta-model shape especially in high and low frequencies. In medium and high frequencies, with a low convergence of non linear residuals, the recirculation length is over-predicted. In low frequencies, the design point with a high amplitude is the most sensitive to this parameter.

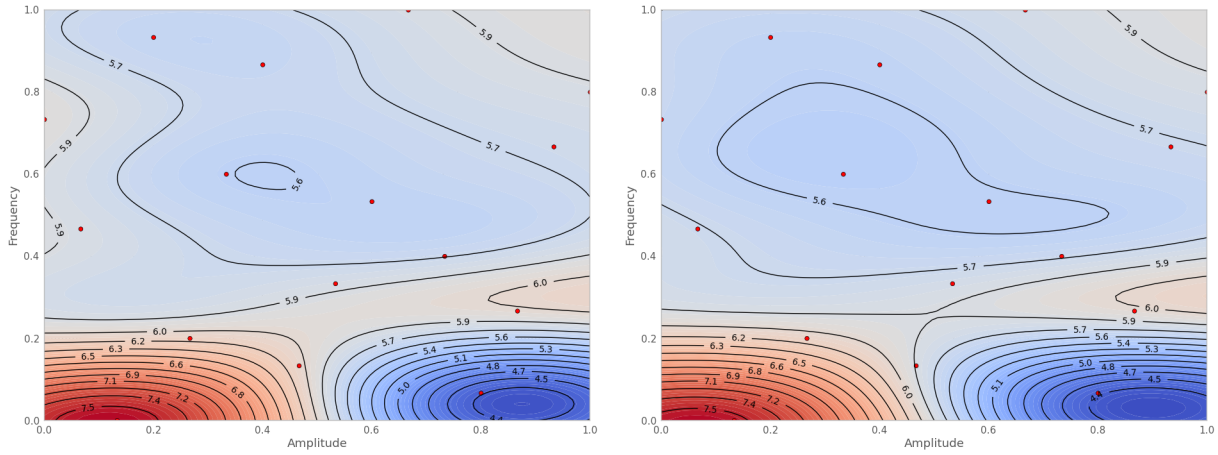

(a) Coarse grid.

(b) Medium grid.

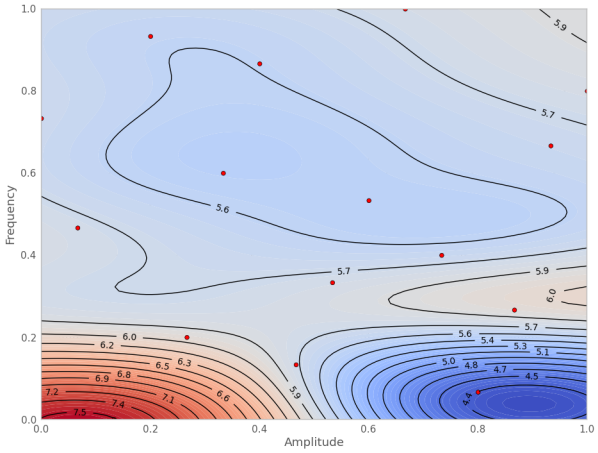

(c) Fine grid.

Figure 7. Grid refinement effect on the recirculation length with kw-ne-easm turbulence closure and 256 time steps by periods.

V.D. Impact of compressibility

Finally, we compare two codes, the incompressible flow solver ISIS-CFD and the compressible flow solver NUM3SIS. The turbulence is modeled by the Spalart-Allmaras closure in both cases, while the fine grid and time step are employed.

The results of these simulations are given on Fig. 10. Similar trends are observed, although the value of the predicted length is different, especially for high frequencies and amplitudes. This behavior may be explained by the fact that compressibility generates a damping effect, especially for high frequencies. The time spent to reach a periodic state from the steady uncontrolled flow is longer for incompressible case. It takes $0.25s$ for the compressible solver against $0.35s$ for the incompressible one.

VI. Impact of simulation parameters on optimization process

Now, we propose to study the effect of simulation parameters on the optimization process. First of all, we show a full optimization using the Spalart-Allmaras model. Then, to overcome some difficulties due to the presence of numerical noise, a filtering approach is proposed and validated with the optimization of an analytical test case, then tested on the Spalart-Allmaras model. Finally an optimization using the k-ω-SST Menter is performed.

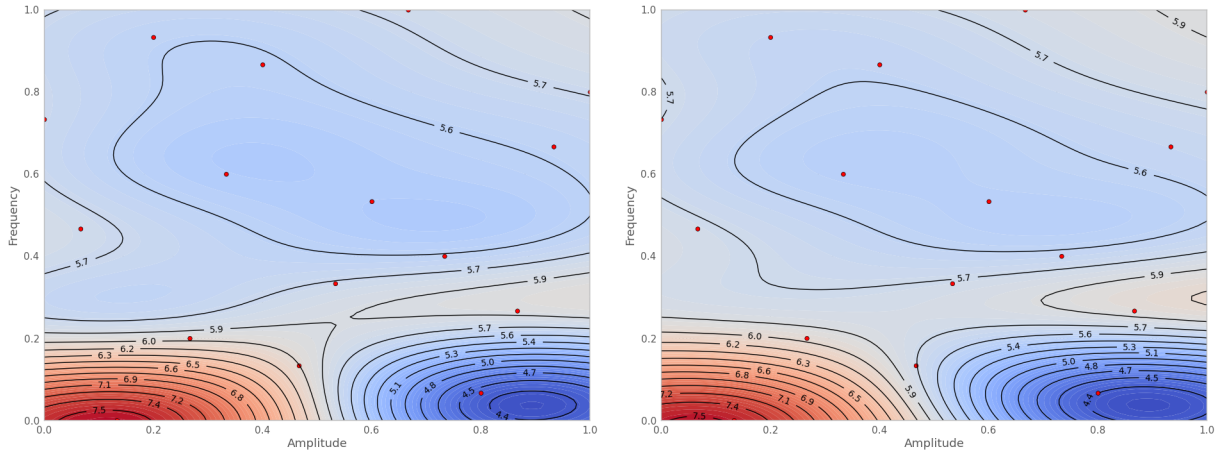

(a) Large time step.

(b) Medium time step.

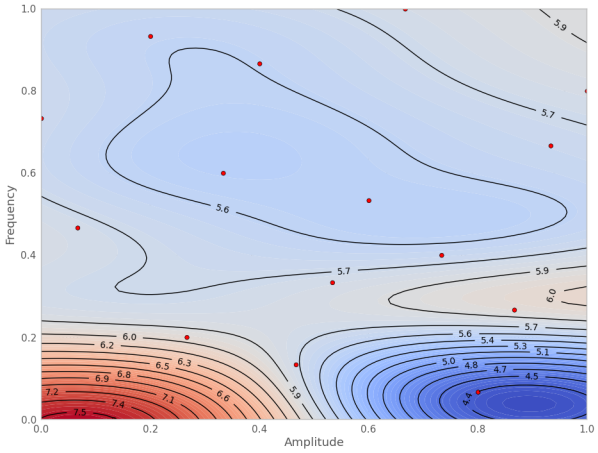

(c) Small time step.

Figure 8. Time step refinement effect on the recirculation length with k-ω-ne-easm turbulence closure and a fine grid and convergence of 4 orders of non linear residuals.

VI.A. Optimization of a synthetic jet with the compressible Spalart-Allmaras model

We consider here the first 9 optimization steps using the lower bound merit function, for the minimisation of the BFS mean flow recirculation length with the compressible code. The turbulence closure is the Spalart-Allmaras model. The initial database contains 15 design points and, for each step, three simulations are run in parallel, so the final database contains 42 points in total. In this case, the recirculation length is computed using the closest grid point for which the friction coefficient vanishes. The mesh used is the coarsest one and the mesh size in the streamwise direction in the recirculation area is $h_{coarse} = 1.10^{-3}m$, which gives a non dimensional size of $h^{adim}_{coarse} = 0.0787$. The Fig. 11 shows the final meta-model obtained with the interpolating meta-model. As seen the model oscillates. Furthermore, by looking at the evaluation points, we see that they are not converging. This indicates that the meta-model changes abruptly each time a new point is added to the database.

VI.B. Optimization with noisy observations

We make the assumption that the oscillations are due to numerical errors yielding a noisy evaluation process. Therefore, we introduce some modification in the Gaussian Process framework to take it into account.

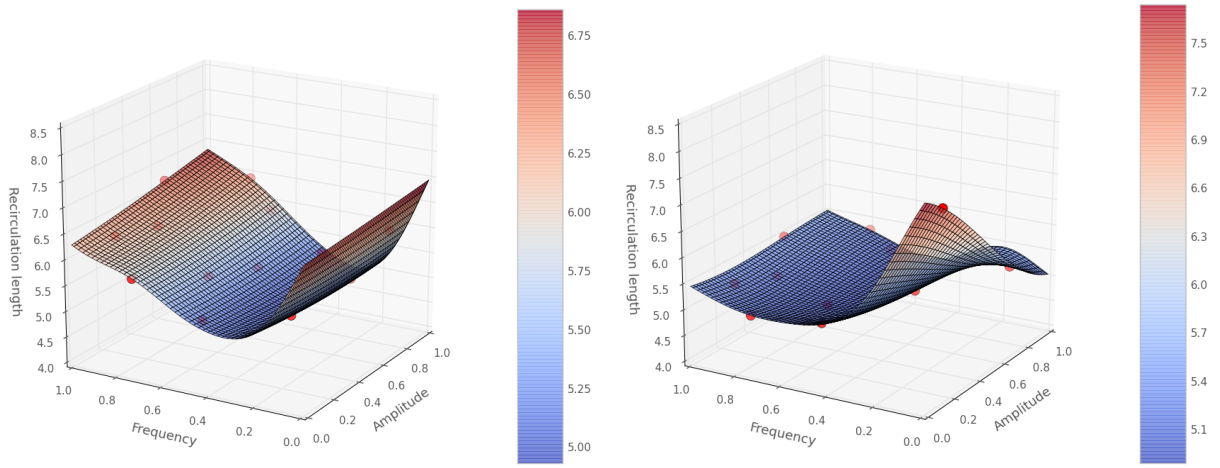

(a) Criterion reduction of 1 order.

(b) Criterion reduction of 2 orders.

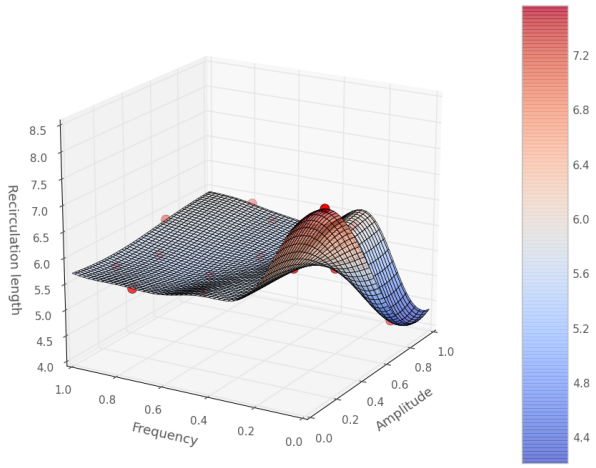

(c) Criterion reduction of 4 orders.

Figure 9. Non linearities convergence criterion effect on the recirculation length with k-ω-ne-easm turbulence closure, a fine grid and a 256 time steps per period.

VI.B.1. Prediction of noisy observations with Gaussian Processes

In real-life problems, either in experiments or numerical simulations, observations made on the process are noisy. In case of experiments, the noise related to gauge or instruments can usually be well estimated. In numerical simulations, errors arise from models, discretization, iterative solvers, human errors, etc. As a consequence, in both cases, we need to take into account noisy observations in our models.

According to Ginsbourger,[36] assuming a Gaussian distributed noise $\boldsymbol{\varepsilon}$, the process observation can be written as:

$$f_\varepsilon(\boldsymbol{x}) = f(\boldsymbol{x}) + \boldsymbol{\varepsilon},$$

with $\varepsilon \sim \mathcal{N}(\mathbf{0}, \Delta)$, where $\Delta = \mathrm{diag}(\tau_i^2, i \in [0, n])$. The error at the observation point i is thus considered as a centered Gaussian distribution with a variance τ_i^2.

By introducing the noise in the process, the variance of the observation C_N is changed to $C_N + \Delta$. As a result, the prediction of mean $\hat{f}_{N+1}$ and variance $\hat{\sigma}^2_{f_{N+1}}$ in Eq. (10) need to be modified to:

$$\hat{f}_{N+1} = \boldsymbol{k_{N+1}}^\top (C_N^{-1} + \Delta)\boldsymbol{F_N}, \qquad \hat{\sigma}^2_{f_{N+1}} = \kappa - \boldsymbol{k_{N+1}}^\top (C_N^{-1} + \Delta)\boldsymbol{k_{N+1}}. \tag{20}$$

In addition, the log-likelihood from Eq. 12 to be minimized becomes:

$$\mathfrak{L} = \frac{1}{2}\boldsymbol{F_N}^T (C_N + \Delta)^{-1} \boldsymbol{F_N} + \frac{1}{2}\log|C_N + \Delta|. \tag{21}$$

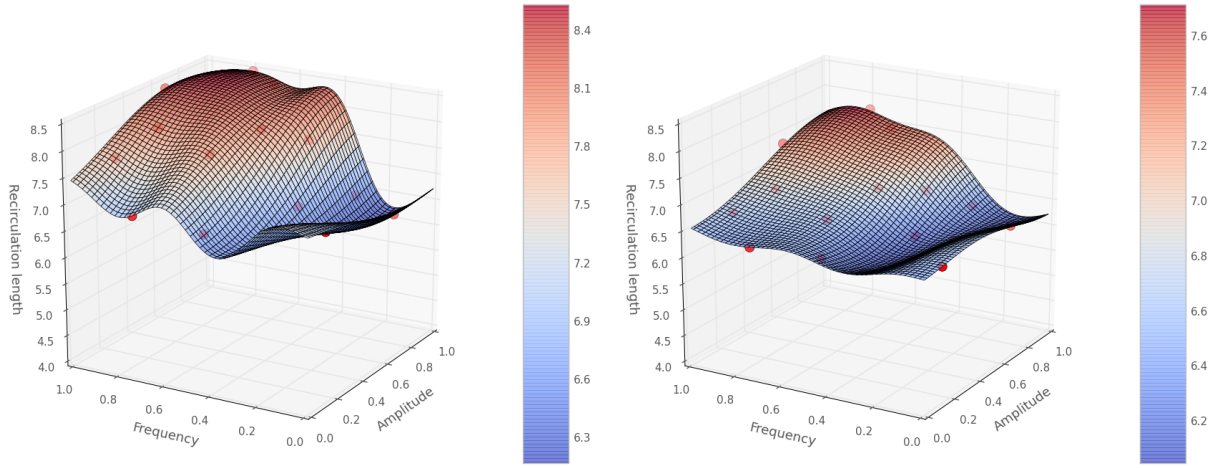

(a) Incompressible ISIS-CFD flow solver. (b) Compressible num3sis flow solver.

Figure 10. Influence of the flow solver on the bubble recirculation length.

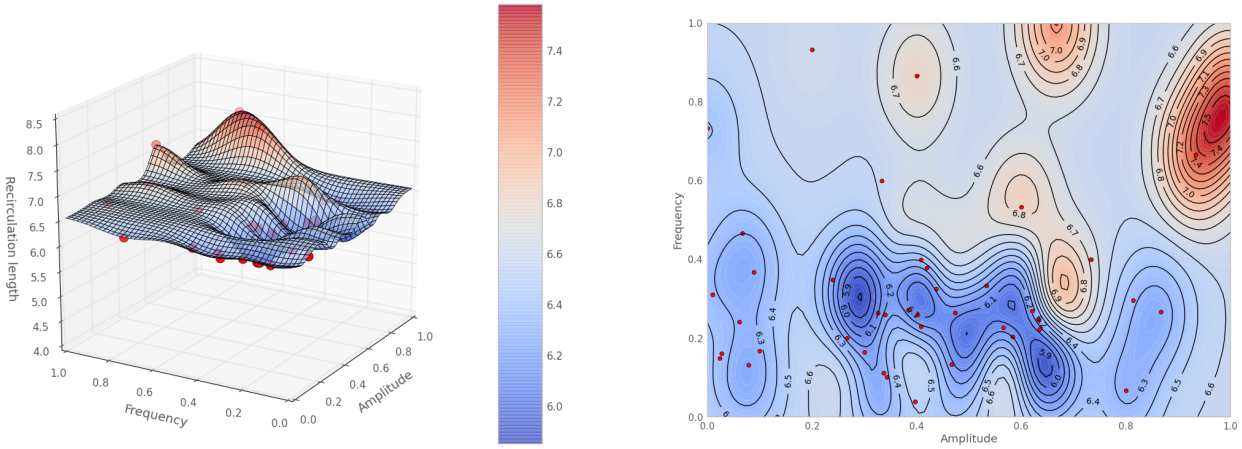

Figure 11. Final interpolating meta-model for the optimization of the recirculation length. The solver is the compressible one with a Spalart-Allmaras closure. For the optimization, we used the lower bound merit function and the final database contains 42 points in total.

VI.B.2. Analytical case

To illustrate the meta-model based optimization of noisy functions, the following unconstrained problem is considered:

$$Minimize \quad f(x) = \frac{1}{2}\left(\frac{\sin(20x)}{1+x} + 3x^3\cos(5x) + 10(x-0.5)^2 - 0.6\right) + \varepsilon_p \tag{22}$$

with $\varepsilon_p \sim \mathcal{N}(0, \tau_p^2)$, a random perturbation with a normal distribution of mean 0 and standard deviation $\tau_p = 0.1$.

Several optimization cases are considered here. The first ones are optimizations using an interpolating meta-model. In that case we consider exact observations. Then, we consider a non interpolating meta-model where the error variance is set to τ_p^2. In all cases, the initial database contains 5 points equally distributed.

Optimization with an interpolating model: An optimization with an interpolating meta-model and an EI merit function is considered. Four figures among the first 15 steps of the optimization are shown on Fig. 12. As we could expect, the optimization of a noisy function using an interpolating meta-model gives a very oscillating model with a strong uncertainty in the low-sampled regions. Whatever the merit function considered, this algorithm would fail to find the global minimum in a limited number of iterations as the

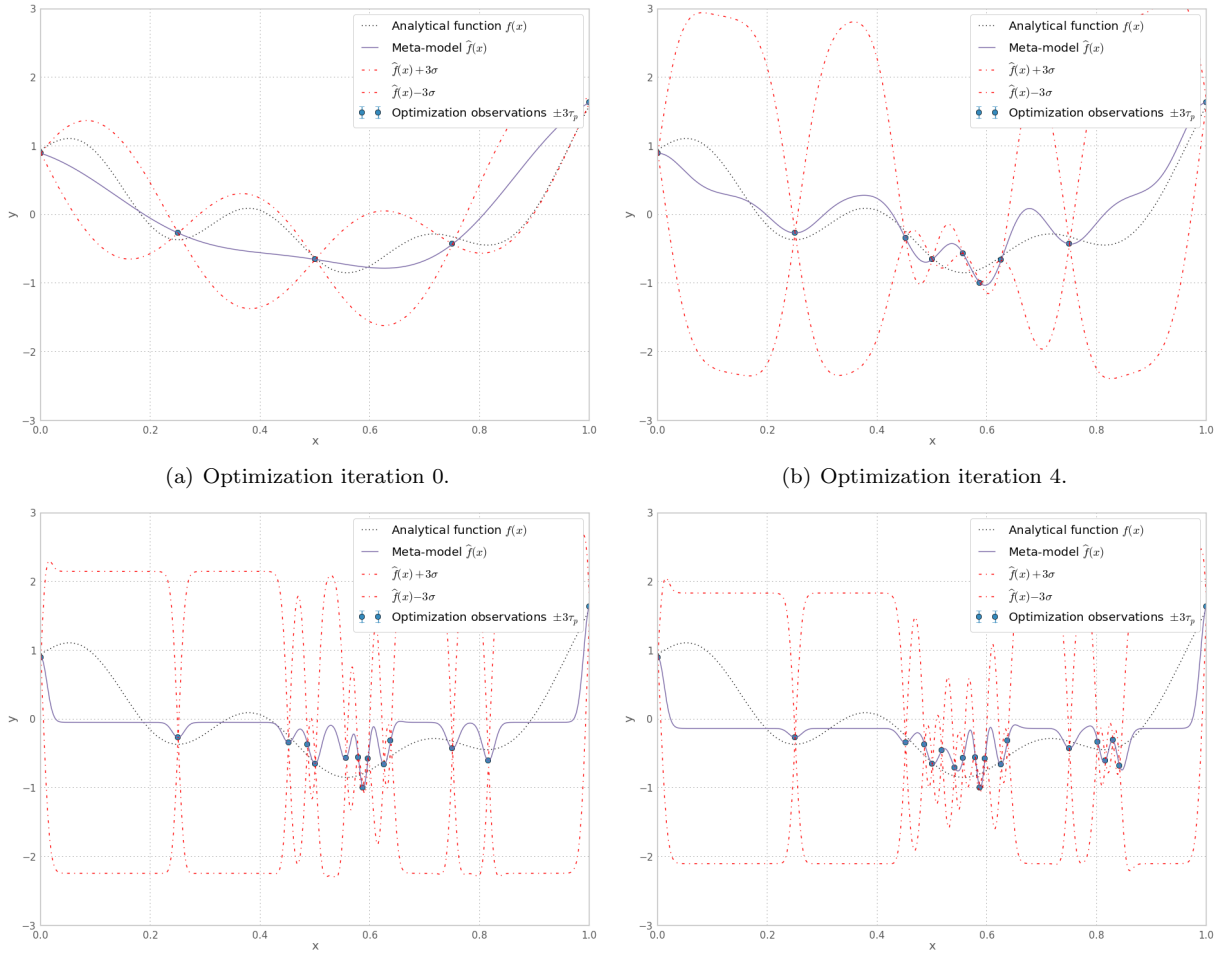

(a) Optimization iteration 0.

(b) Optimization iteration 4.

(c) Optimization iteration 9.

(d) Optimization iteration 14.

Figure 12. Optimization with the expected improvement of a 1D function using $\tau_p = 0.1$ and an interpolating meta-model.

meta-model is too far from the reality.

Optimization with a non interpolating model: As previously seen, increasing the points in the database for a noisy function yields an oscillating meta-model. To address this problem, we consider here the meta-model including noisy observations.

First, an optimization with a non-interpolating meta-model with the EI merit function is considered. Four steps among the 15 optimization iterations are shown on Fig. 13. These figures show that the meta-model converges to the global minimum. Furthermore, as the number of iteration increases, the meta-model remains stable, which is not the case with an interpolating meta-model.

VI.B.3. Application to the CFD case

We reconsider the final database of the section VI.A and construct non-interpolating meta-models with different level of error. Fig. 14 shows that the oscillating model becomes more stable as the error standard deviation is increased. $3\tau_i \approx h_{coarse}^{adim} = 0.0787$ seems to be a threshold value, indicating that the error is related to the cell size at reattachment point.

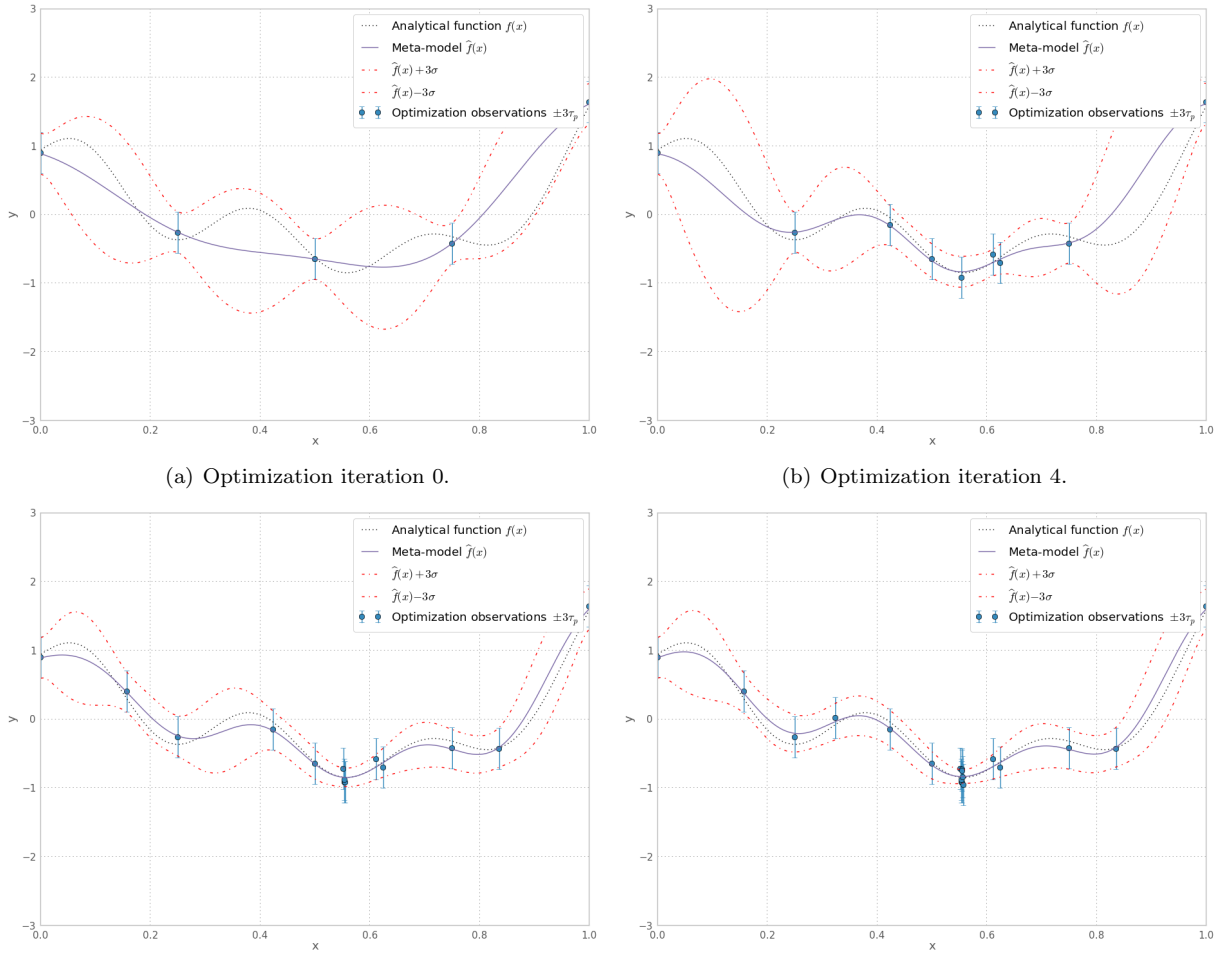

(a) Optimization iteration 0.

(b) Optimization iteration 4.

(c) Optimization iteration 9.

(d) Optimization iteration 14.

Figure 13. Optimization with the expected improvement of a 1D function using $\tau_p = 0.1$ and non-interpolating meta-model, with an observation uncertainty standard deviation set to $\tau_i = 0.1$.

VI.C. Optimization of a synthetic jet with the incompressible k-ω-SST Menter model

In the following, we examine the optimization of synthetic jet parameters using the k-ω-SST Menter model since this model seems to provide a more reliable flow prediction. The initial database is composed of 6 design points selected using an optimized Latin Hypercube Sampling algorithm. 128 time steps per period and a reduction of non linear residuals of 3 orders are chosen. The initial database is represented on the Fig. 15. The meta-model after six iterations using PI and AEI merit functions are shown on Fig. 16. During the first iterations, the method based on PI tends to concentrate the points around the located optimum yielding oscillatory behavior as section VI.B.3. On the contrary, the method based on AEI begins to spread the points in the research domain avoiding the oscillatory effect during the first phase of the optimization.

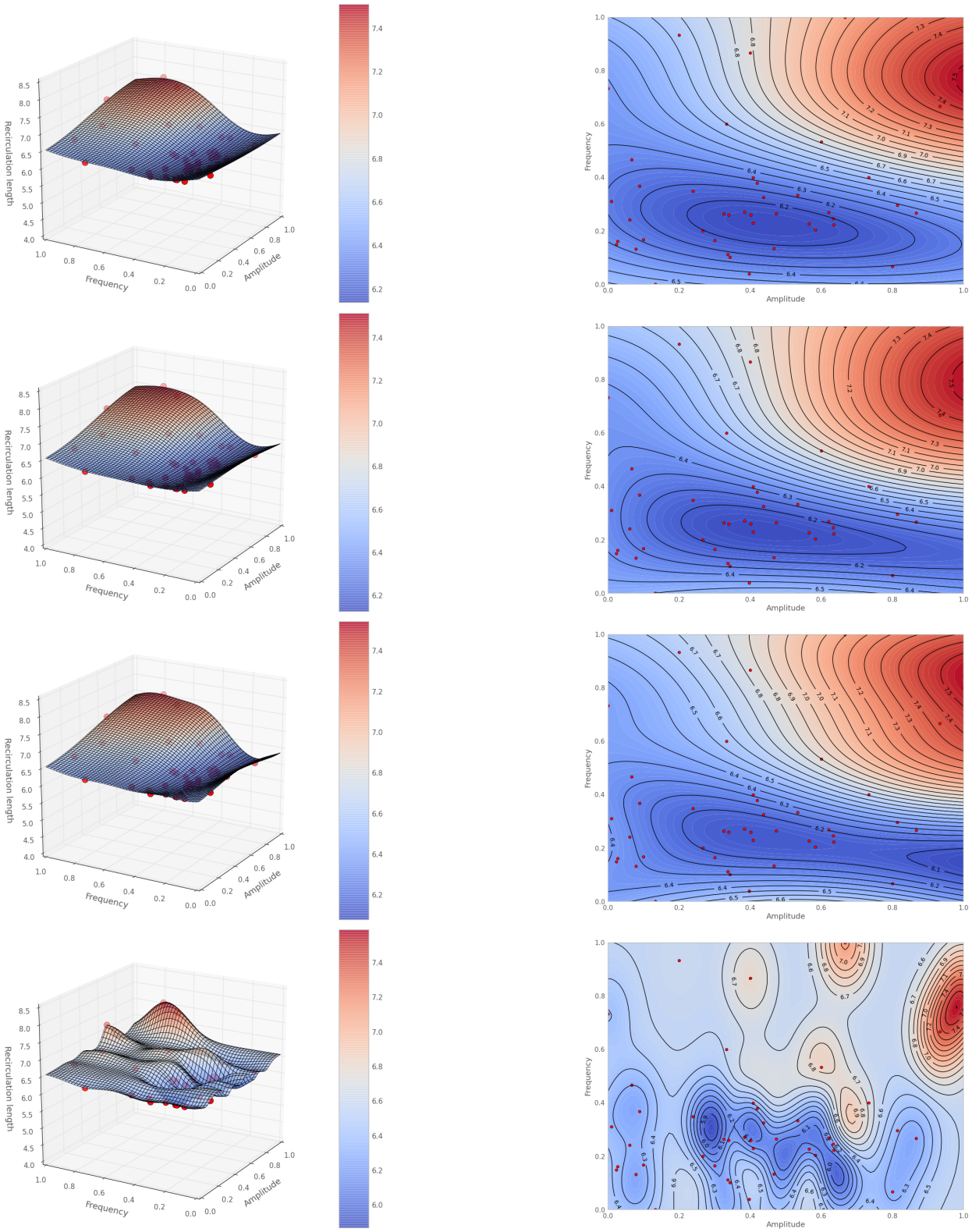

Figure 14. Comparison of meta-models using the same database coming from an optimization with different level of standard deviation to model the error. From the top to the bottom, $\tau_i = 0.1, \tau_i = 0.05, \tau_i = 0.02, \tau_i = 0.01$. As the standard deviation of the error decreases, the meta-model becomes unstable due to the presence of noise in the observations.

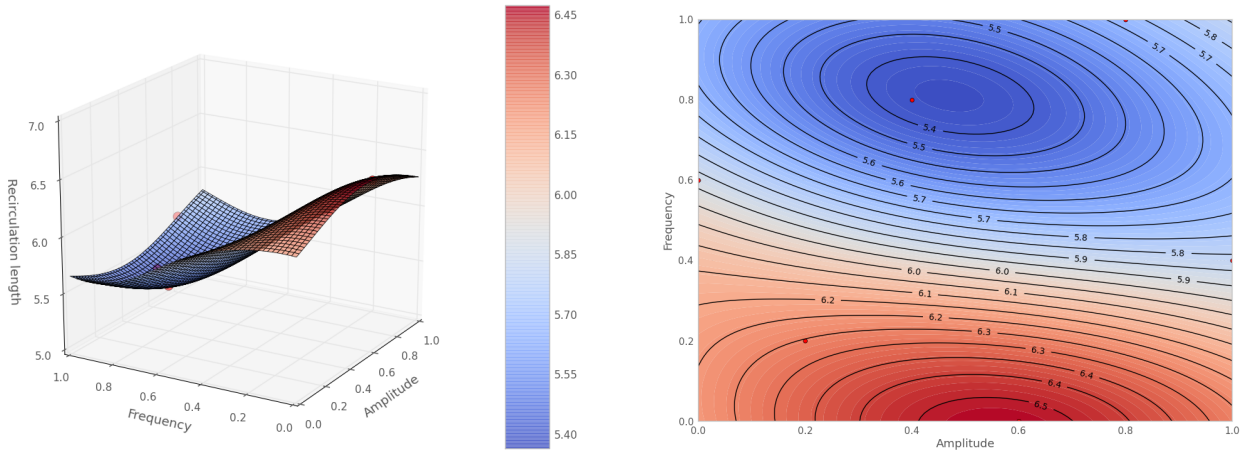

Figure 15. Initial database generated for the optimization of jet amplitude and frequency. The k-ω-SST Menter model, 128 time steps per period and a reduction of non linear residuals of 3 orders is used.

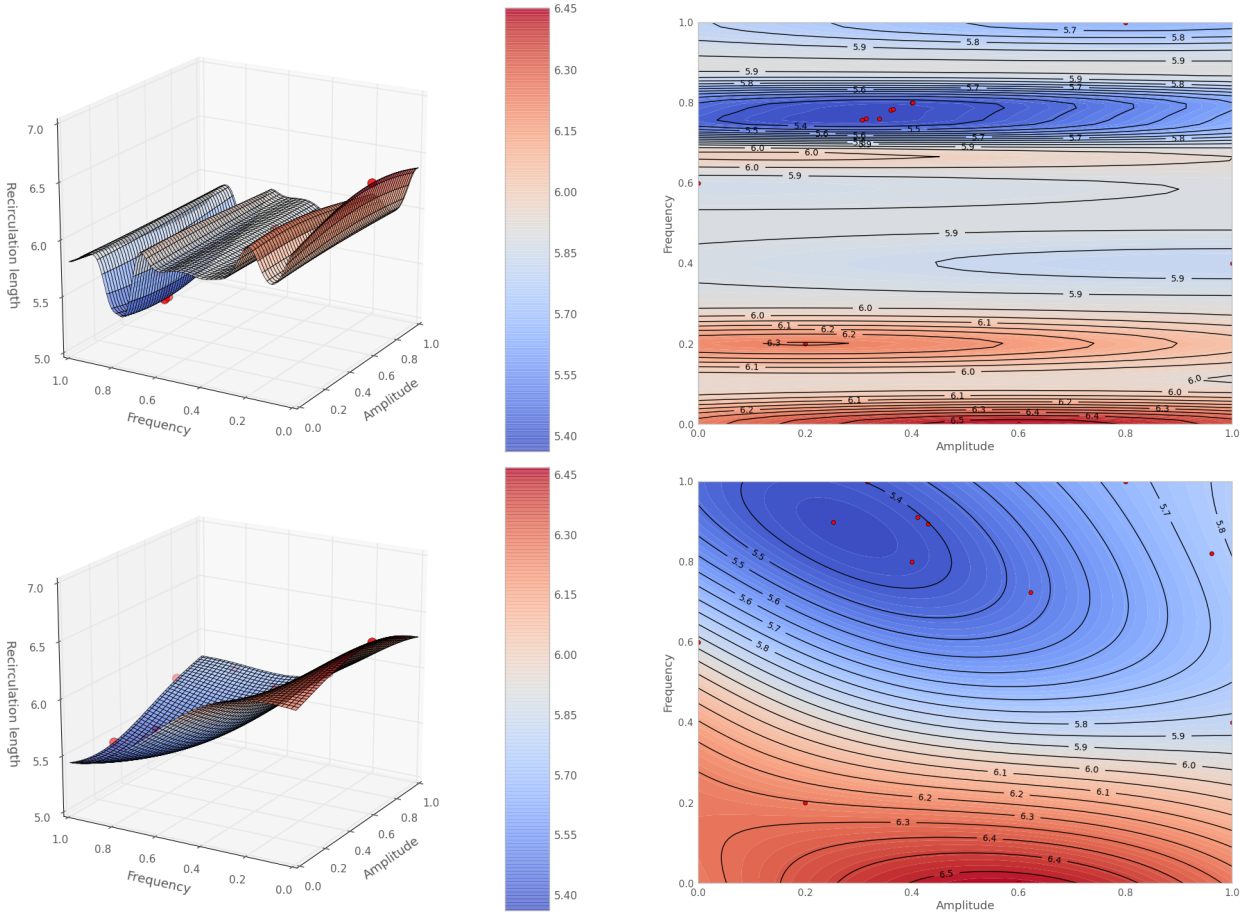

Figure 16. Comparison of meta-models after five optimization iterations of jet amplitude and frequency parameters using PI and AEI. The k-ω-SST Menter model, 128 time steps per period and a reduction of non linear residuals of 3 orders is used. The PI (top), AEI (bottom) merit functions are used.

VII. Conclusion and prospects

In this study, we have first analysed the effect of numerical parameters and turbulence modeling on the controlled flow over a backward facing step using a design of experiment approach. The grid size and time step have not a significant impact on the response surface for the computation carried out here. The most critical numerical parameter is the non linear residual reduction criterion which dramatically modifies the recirculation length. On the other side, the most significant influence on the response surface is due to the turbulence closure. The Spalart-Allmaras model gives an efficient control for high amplitude and low frequency, while the k-ω-SST Menter tends to give good control parameters at mid-frequency and mid-amplitude. The behavior of the k-ω-ne-easm agrees for the mid-range parameters with the k-ω-SST Menter model, but it presents some different characteristics at high amplitude and low frequency jet parameters.

Moreover, the necessity to account for numerical error during the meta-model based optimization has been shown. In particular, the use of interpolating models yields oscillating and unrealistic representations, leading the optimization process to failure. The introduction of the noisy observation concept allowed to overcome this difficulty. In the test case considered here, the noise level seems to be related to the grid size at reattachment point

The question how to automatically estimate the numerical error made on each point still remains. This question has been studied by Forrester et al.[37] and more sophisticated approached will be investigated in the future.

Acknowledgments

This study is partially supported by the 7th Framework Program of the European Union, project number 266326 "MARS".

References

[1]Donovan, J., Kral, L., and Cary, A., "Active flow control applied to an airfoil," AIAA Paper 98–0210, January 1998.

[2]Ekaterinaris, J., "Active flow control of wing separated flow," ASME FEDSM'03 Joint Fluids Engineering Conference, Honolulu, Hawai, USA, July 6-10, 2003.

[3]Bergmann, M. and Cordier, L., "Optimal control of the cylinder wake in the laminar regime by trust-region methods and POD reduced-order models," *J. Comput. Physics*, Vol. 227, No. 16, 2008.

[4]Duvigneau, R. and Visonneau, M., "Optimization of a synthetic jet actuator for aerodynamic stall control," *Computers and Fluids*, Vol. 35, July 2006, pp. 624–638.

[5]He, J. W., Glowinski, R., Metcalfe, R., Nordlander, A., and Periaux, J., "Active Control and Drag Optimization for Flow Past a Circular Cylinder: I. Oscillatory Cylinder Rotation," *Journal of Computational Physics*, Vol. 163, No. 1, 2000, pp. 83 – 117.

[6]Carnarius, A., Thiele, F., Oezkaya, E., Nemili, A., and Gauger, N., "Optimization of active flow control of a NACA 0012 airfoil by using a continuous adjoint approach," *European Congress on Computational Methods in Applied Sciences and Engineering, Vienna, Austria*, 2012.

[7]Zymaris, A., Papadimitriou, D., Giannakoglou, K., and Othmer, C., "Optimal location fo suction or blowing jets using the continuous adjoint approach," *European Congress on Computational Methods in Applied Sciences and Engineering ECCOMAS 2010 Lisbon*, 2010.

[8]Duvigneau, R., Hay, A., and Visonneau, M., "Optimal location of a synthetic jet on an airfoil for stall control," *Journal of Fluid Engineering*, Vol. 129, No. 7, July 2007, pp. 825–833.

[9]Batten, P., Clarke, N., Lambert, C., and Causon, M., "On the choice of wavespeeds for the HLLC Riemann solver," *SIAM J. Sci. Comput.*, Vol. 18, No. 6, November 1997, pp. 1553–1570.

[10]Kloczko, T., Corre, C., and Beccantini, A., "Low-cost implicit schemes for all-speed flows on unstructured meshes," *International Journal for Numerical Methods in Fluids*, Vol. 58, No. 5, October 2008, pp. 493–526.

[11]Jasak, H., *Error Analysis and Estimation for the Finite Volume Method with Applications to Fluid Flows*, Ph.D. thesis, Department of Mechanical Engineering, June 1996.

[12]Queutey, P. and Visonneau, M., "An interface capturing method for free-surface hydrodynamic flows," *Computers & fluids*, Vol. 36, No. 9, 2007, pp. 1481–1510.

[13]Duvigneau, R., Visonneau, M., and Deng, G., "On the role played by turbulence closures in hull shape optimization at model and full scale," *Journal of marine science and technology*, Vol. 8, No. 1, 2003, pp. 11–25.

[14]RHIE, C., *A numerical study of the turbulent flow past an isolated airfoil with trailing edge separation*, American Institute of Aeronautics and Astronautics, 2012/11/20 1963.

[15]Dwight, R., *Efficiency improvements of RANS-based analysis and optimization using implicit and adjoint methods on unstructured grids*, Ph.D. thesis, the University of Manchester, 2006.

[16]SPALART, P. and ALLMARAS, S., "A one-equation turbulence model for aerodynamic flows," *AIAA, Aerospace Sciences Meeting and Exhibit, 30 th, Reno, NV*, 1992, p. 1992.

[17]Launder, B. and Spalding, D., "The numerical computation of turbulent flows," *Computer Methods in Applied Mechanics and Engineering*, Vol. 3, No. 2, 1974, pp. 269 – 289.

[18]Menter, F., "Zonal two-equation k-omega turbulence models for aerodynamic flows," *AIAA Journal*, 1993.

[19]Carpy, S. and Manceau, R., "Turbulence modelling of statistically periodic flows: Synthetic jet into quiescent air," *International Journal of Heat and Fluid Flow*, Vol. 27, No. 5, 2006, pp. 756 – 767.

[20]Gatski, T. and Speziale, C., "On explicit algebraic stress models for complex turbulent flows," *Journal of Fluid Mechanics*, Vol. 254, No. 1, 1993, pp. 59–78.

[21]Deng, G. and Visonneau, M., "Comparison of explicit algebraic stress models and second-order turbulence closures for steady flows around ships," *Proc. 7th Int. Conf. on Numerical Ship Hydrodynamics, Nantes, France*, 1999.

[22]Labroquère, J. and Duvigneau, R., "Optimization Methods Applied to Aerodynamic Flow Control," *ECCOMAS - European Congress on Computational Methods in Applied Sciences and Engineering - 2012*, edited by J. E. et.al., VIenna, Autriche, Sept. 2012.

[23]Duvigneau, R. and Chandrashekar, P., "Kriging-based optimization applied to flow control," *International Journal for Numerical Methods in Fluids*, Vol. 69, No. 11, Aug. 2012, pp. 1701–1714.

[24]Jones, D., Schonlau, M., and Welch, W., "Efficient global optimization of expensive black-box functions," *Journal of Global optimization*, Vol. 13, No. 4, 1998, pp. 455–492.

[25]Gibbs, M. and MacKay, D., "Efficient implementation of Gaussian processes," 1997.

[26]MacKay, D., "Bayesian interpolation," *Neural computation*, Vol. 4, No. 3, 1992, pp. 415–447.

[27]Jones, D., "A taxonomy of global optimization methods based on response surfaces," *Journal of Global Optimization*, Vol. 21, No. 4, 2001, pp. 345–383.

[28]Huang, D., Allen, T., Notz, W., and Zeng, N., "Global optimization of stochastic black-box systems via sequential kriging meta-models," *Journal of Global Optimization*, Vol. 34, No. 3, 2006, pp. 441–466.

[29]Picheny, V., Wagner, T., and Ginsbourger, D., "A benchmark of kriging-based infill criteria for noisy optimization," .

[30]Driver, D. and Seegmiller, H., "Features of a reattaching turbulent shear layer in divergent channel flow," *AIAA journal*, Vol. 23, No. 2, 1985, pp. 163–171.

[31]Le, H., Moin, P., and Kim, J., "Direct numerical simulation of turbulent flow over a backward-facing step," *Journal of Fluid Mechanics*, Vol. 330, No. 1, 1997, pp. 349–374.

[32]Yoder, D. and Georgiadis, N., *Implementation and Validation of the Chien K-[epsilon] Turbulence Model in the Wind Navier-Stokes Code*, National Aeronautics and Space Administration, Glenn Research Center, 1999.

[33]Rumsey, C. and Thomas, J., "Application of FUN3D and CFL3D to the Third Workshop on CFD Uncertainty Analysis," *Proceedings of the 3rd Workshop on CFD Uncertainty Analysis*, 2008.

[34]Labroquère, J. and Duvigneau, R., "Optimization methods applied to aerodynamic flow control," *European Congress on Computational Methods in Applied Sciences and Engineering, Vienna, Austria*, September 2012.

[35]Eça, L., Hoekstra, M., Roache, P., and Coleman, H., "Code verification, solution verification and validation: an overview of the 3rd Lisbon workshop," Tech. rep., AIAA-2009-0047 (June 2009), 2009.

[36]Ginsbourger, D., *Multiples métamodèles pour l'approximation et l'optimisation de fonctions numériques multivariables*, Ph.D. thesis, École Nationale Supérieure des Mines de Saint-Étienne, March 2009.

[37]J. Forrester, A. I., Keane, A. J., and Bressloff, N. W., "Design and analysis of" noisy" computer experiments," *AIAA journal*, Vol. 44, No. 10, 2006, pp. 2331–2339.